

Discrete Breathers in a Realistic Coarse-Grained Model of Proteins

Stefano Luccioli^{1,2,3}, Alberto Imparato⁴, Stefano Lepri^{1,2},
Francesco Piazza⁵ and Alessandro Torcini^{1,2,3,4}

¹ CNR - Consiglio Nazionale delle Ricerche, Istituto dei Sistemi Complessi, via Madonna del Piano 10, I-50019 Sesto Fiorentino, Italy

² Centro Interdipartimentale per lo Studio delle Dinamiche Complesse, via G. Sansone, 1 - I-50019 Sesto Fiorentino, Italy

³ Istituto Nazionale di Fisica Nucleare, Sez. Firenze, via G. Sansone, 1 - I-50019 Sesto Fiorentino, Italy

⁴Dept. of Physics and Astronomy, University of Aarhus, Ny Munkegade, Building 1520 - DK-8000 Aarhus C, Denmark

⁵Université d'Orléans and Centre de Biophysique Moléculaire, (CBM-CNRS), Rue Charles Sadron, 45071 Orléans Cedex, France

Abstract. We report the results of molecular dynamics simulations of an off-lattice protein model featuring a physical force-field and amino-acid sequence. We show that localized modes of nonlinear origin (discrete breathers) emerge naturally as continuations of a subset of high-frequency normal modes residing at specific sites dictated by the native fold. In the case of the small β -barrel structure that we consider, localization occurs on the turns connecting the strands. At high energies, discrete breathers stabilize the structure by concentrating energy on few sites, while their collapse marks the onset of large-amplitude fluctuations of the protein. Furthermore, we show how breathers develop as energy-accumulating centres following perturbations even at distant locations, thus mediating efficient and irreversible energy transfers. Remarkably, due to the presence of angular potentials, the breather induces a local static distortion of the native fold. Altogether, the combination of this two nonlinear effects may provide a ready means for remotely controlling local conformational changes in proteins.

PACS numbers: 87.15.A-,05.45.-a,63.20.Pw

Submitted to: *Phys. Biol.*

1. Introduction

Biopolymers such as proteins and nucleic acids fold into complex three-dimensional structures, whose shape is strictly connected to their biological function [1]. The conformation of such molecules can change dynamically, in turn modulating the function: for example, activation or inactivation of enzymes relies on specific structural modifications occurring at specific locations [2, 3, 4]. Typically, such changes are driven by either mechanical forces or by converting chemical energy into conformational rearrangements and thus into mechanical work.

Proteins in physiological conditions are immersed in a thermal bath and therefore exhibit random thermal fluctuations. However, the biological function of a given biopolymer is often closely related to a particular kind of motion, typically involving large-scale vibrations [5, 6, 7, 8, 9] or the fluctuations of entire hinge-domain units [10, 11, 12, 13].

If collective, low-frequency modes have been traditionally assumed to describe functional patterns, there is growing evidence that high-frequency vibrations contain information on protein stability [14]. Importantly, fast modes are strongly localized, due to the geometric heterogeneity of protein structures. Typically, such vibrations are localized at extremely stiff regions, such as hinges, which in turn assume a prominent role in regulating protein stability and function, as also suggested by experiments [4]. It is also known that active sites of enzymes have a marked tendency to be located within the stiffest segments of the structures [15, 16], which provides a further intriguing motivation to investigate the connection between localized vibrations and the peculiarities of protein folds.

When nonlinear effects are considered, the connection between the dynamics of localized modes and the details of the scaffolds becomes more interesting. Recently, it has been shown that band-edge normal modes (NMs) can be continued to nonlinear localized vibrations of high energy termed Discrete Breathers (DBs) [15], also known as intrinsic localized modes [17]. DBs are time-periodic, spatially localized solutions emerging generically in discrete networks of nonlinear oscillators [18, 19], that have been also observed experimentally in many systems [19, 20, 21, 22].

While DBs have been widely studied in spatially homogeneous systems [19], the role played by inhomogeneity on their properties remains largely unknown. However, the dynamical behaviours of DBs discovered so far in protein models are remarkable. In the context of the nonlinear network model (NNM), it has been shown that DBs emerge spontaneously, upon surface cooling, at few specific sites, invariably within the stiffest regions [23]. Moreover, they are also able to self-excite at a target site upon injecting some energy at a different location, thus mediating high-yield energy transfer events [24, 25, 26]. In a more simplified model, it has been shown that DB excitation lowers the free-energy barrier associated with a given enzyme-catalyzed reaction [27], thus confirming the role of protein dynamics in reaction-rate enhancement by enzymes highlighted by recent experiments [28].

However, DBs in proteins have only been found and characterized so far in extremely simplified models, either taking into account the three-dimensional folds but with no heterogeneity in the force constants [15], or with slightly more elaborate potentials but imposing crudely simplified geometries [29, 30, 31]. Importantly, all studies performed so far notably lacked (i) realistic inter-particle potentials and (ii) an explicit account of the amino acid sequence. In this paper, we make a step forward by investigating DB excitation and their properties in a realistic off-lattice model of protein dynamics with coarse-grained realistic interaction potentials and a three-code amino-acid sequence.

The paper is organized as follows. In the next section we introduce our system and describe the model, along with an account of our simulation and analysis protocols. In section 3, we describe the emergence of DBs as numerical continuation of NMs and provide a thorough characterization of their properties. Finally, we summarize our findings and outline possible future directions prompted by our results.

2. Model and numerical methods

The 3D off-lattice protein model studied in this paper is a modified version of the one initially introduced in Ref. [32] and successively generalized to include a harmonic interaction between next-neighbouring beads instead of rigid bonds [33]. This model has been studied to describe thermally-driven folding and unfolding [32, 34, 35, 33, 36, 37, 38, 39] and, more recently, to reproduce mechanical manipulation experiments [40, 41, 42, 43, 44, 45]. It consists of a chain of L point-like monomers mimicking the residues of a polypeptidic chain with an associated aminoacid sequence coded by a three-letter alphabet: hydrophobic (B), polar (P) and neutral (N). The intramolecular potential consists of four terms: a stiff nearest-neighbour harmonic potential, V_H , intended to maintain the bond distance almost constant, a three-body interaction V_A , which accounts for the energy associated with bond angles, a four-body interaction V_D corresponding to the dihedral angle potential, and a long-range Lennard-Jones (LJ) interaction, V_{LJ} , acting on all pairs i, j such that $|i - j| > 2$, namely

$$V_H(r_{i,i+1}) = \alpha(r_{i,i+1} - r_0)^2 \quad (1)$$

$$V_A(\theta_i) = A \cos(\theta_i) + B \cos(2\theta_i) - V_0 \quad (2)$$

$$V_D(\varphi_i, \theta_i, \theta_{i+1}) = C_i [1 - S(\theta_i, \theta_{i+1}) \cos(\varphi_i)] \\ + D_i [1 - S(\theta_i, \theta_{i+1}) \cos(3\varphi_i)] \quad (3)$$

$$V_{LJ}(r_{i,j}) = \varepsilon_{i,j} \left(\frac{1}{r_{i,j}^{12}} - \frac{c_{i,j}}{r_{i,j}^6} \right) \quad (4)$$

Here, $r_{i,j}$ is the distance between the i -th and the j -th monomer, while θ_i and φ_i are the bond and dihedral angles at the i -th monomer, respectively. The parameters α and $r_0 = 1$ fix the strength and the equilibrium distance between consecutive monomers along the backbone, respectively. The term $V_A(\theta_i)$ is such that it corresponds, up to the

second order, to a harmonic term $k_\theta(\theta_i - \theta_0)^2/2$, where

$$A = -k_\theta \frac{\cos \theta_0}{\sin^2 \theta_0}, \quad B = \frac{k_\theta}{4 \sin^2 \theta_0},$$

$$V_0 = A \cos \theta_0 + B \cos(2\theta_0) \quad ,$$

with $k_\theta = 20$, $\theta_0 = 5\pi/12$ rad or 75° [46].

The dihedral-angle potential is characterized by three minima for $\varphi = 0$ (associated with the so-called *trans* state) and $\varphi = \pm 2\pi/3$ (corresponding to *cis* states). This term is mainly responsible for the formation of secondary structures. In particular, large values of the parameters C_i, D_i favor the formation of the *trans* state and therefore of β -sheets, while when *cis* states prevail α -helices are formed. The parameters (C_i, D_i) have been chosen as in Ref. [36], *i.e.* if two or more beads among the four defining φ are neutral (N) then $C_i = 0$ and $D_i = 0.2$, in all the other cases $C_i = D_i = 1.2$. The *tapering function* $S(\theta_i, \theta_{i+1})$ has been introduced in the expression of V_D in order to smooth off the singularities introduced by the derivatives of the dihedral angle cosines (for an exact definition see Refs. [43, 47]).

The Lennard-Jones term V_{LJ} describes the interactions with the solvent, that depend on the nature of the interacting residues as follows: if any of the two monomers is neutral, the potential is repulsive $c_{N,X} = 0$ and its energy scale is fixed by $\varepsilon_{N,X} = 4$; for interactions between hydrophobic residues $c_{B,B} = 1$ and $\varepsilon_{B,B} = 4$; for any polar-polar or polar-hydrophobic interaction $c_{P,P} \equiv c_{P,B} = -1$ and $\varepsilon_{P,P} \equiv \varepsilon_{P,B} = 8/3$.

According to the above definitions, the Hamiltonian of the system reads

$$H = K + V = \sum_{i=1}^L \frac{|\vec{p}(i)|^2}{2} + \sum_{i=1}^{L-1} V_H(r_{i,i+1}) +$$

$$+ \sum_{i=2}^{L-1} V_A(\theta_i) + \sum_{i=2}^{L-2} V_D(\varphi_i, \theta_i, \theta_{i+1}) + \sum_{i=1}^{L-3} \sum_{j=i+3}^L V_{LJ}(r_{ij}) \quad (5)$$

where all monomers are assumed to have the same unitary mass.

In the present paper we consider the following sequence of $L = 46$ monomers: $B_9N_3(PB)_4N_3B_9N_3(PB)_5P$. This sequence has been widely analyzed in the past for thermal folding [32, 34, 35, 36, 33, 37, 38, 39] as well as for mechanically induced unfolding and refolding [40, 41, 42, 43]. Here, we adopt the same potential and parameters as in Refs. [36, 42, 43], except for a stiffer harmonic constant α ($50 \leq \alpha \leq 1000$). The simulations reported henceforth refer to $\alpha = 1000$, except when otherwise indicated. We have verified that this choice does not affect the thermodynamic properties of the model (*i.e.* the *folding temperature* and the *hydrophobic collapse temperature*) found in Ref. [43] for $\alpha = 50$. This result could be expected, since the harmonic bead-bead interaction introduced in [33] has been already shown not to alter the folding properties of the original Honeycutt-Thirumalai model [32].

With the above choice of parameters, the heteropolymer exhibits a four-stranded β -barrel native configuration (NC), described by the coordinates $\vec{q}_{NC}(i)$, $i = 1 \dots L$, and shown in Fig. 1. The NC corresponds to the absolute minimum of the potential energy, whose value for $\alpha = 1000$ is $V_{NC} \approx -48.94$. The native structure is stabilized by the

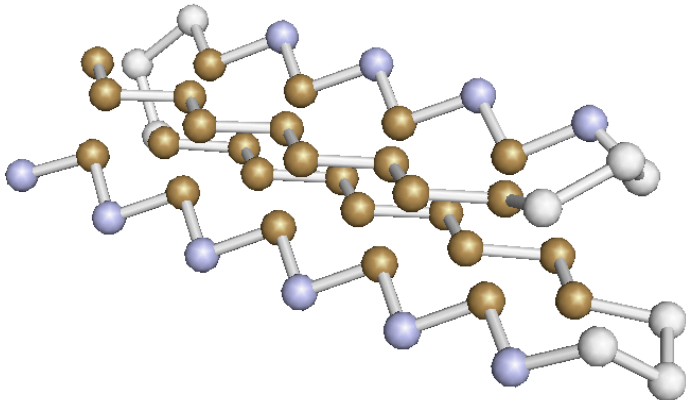


Figure 1. (Color online) Native configuration of the protein model. Different colors represent the three different types of beads: white (neutral), light blue (polar) and sand (hydrophobic). Parameters are: $L = 46$, $\alpha = 1000$.

attractive hydrophobic interactions among the B residues, in particular the first and third B_9 strands, forming the core of the NC, are parallel to each other and anti-parallel to the second and fourth strand $(PB)_4$ and $(PB)_5P$. The latter are exposed to the solvent due to the presence of polar residues. Overall, the four strands are separated by stretches of three consecutive neutral beads, forming as many turns (see Fig. 1). These involve the following sites: 10-12 (first turn), 21-23 (second turn) and 33-35 (third turn).

In the following, we report equilibrium microcanonical results obtained by integrating Hamilton's equations by means of a fourth order symplectic integrator [48] with a time-step of 10^{-3} time units (ensuring a relative energy conservation of $\sim 10^{-7}$). In all cases, the initial coordinates of the beads were taken to correspond to the NC (zero-displacement).

2.1. Normal modes analysis

The properties of nonlinear modes in spatially and force-heterogeneous systems strongly depend on the features of the linear spectrum: in particular, non-resonant nonlinear modes may emerge within inter-mode gaps and highly localized vibrations can be associated with band edges [15]. Hence, a detailed understanding of the linear spectrum is an essential pre-requisite for our analysis. More precisely, we wish to investigate how the normal mode frequencies and eigenvectors depend on the harmonic bond stiffness α .

The NM spectrum associated with the NC of our model protein is composed by $3L - 6$ non-zero frequencies $\{f_k = \sqrt{\lambda_k}/2\pi\}$, λ_k , being the eigenvalues of the Hessian matrix [49]. The NM spectra are reported in Fig. 2 (a) for values of α ranging from 50 to 1000. The most important observation for our purposes is that, for large enough values

of α , the spectrum splits in two bands separated by a gap. The highest portion (the optical band) comprises $L - 1$ modes associated with the stiffest force constants, that is bond (backbone) distortions along the chain, while the lowest part (the acoustic band) is composed by the remaining $2L - 5$ modes that represent collective motions of the beads which are hardly affected by changes in α . This interpretation can be substantiated by the following analysis. We have first slightly perturbed the NC along the direction of each eigenvector with an arbitrary amplitude ε , *i.e.* $\vec{q}_{NC}(i) \rightarrow \vec{q}_k(i) = \vec{q}_{NC}(i) + \varepsilon \vec{e}_k(i)$. Then we have evaluated the relative variations of the potential energy components V_j , $j = H$ (harmonic), A (three-body angular), D (dihedral), LJ (Lennard-Jones), with respect to their values in the NC according to the following definition:

$$\Delta_{k,V_j} = \frac{|V_j(\vec{q}_k) - V_j(\vec{q}_{NC})|}{|V_j(\vec{q}_k)|}, \quad (6)$$

As it is clear from Fig. 3, the perturbation along the first 45 eigenvectors is only restricted to the degrees of freedom associated with bond deformation, *i.e.* to the harmonic contribution to the potential energy.

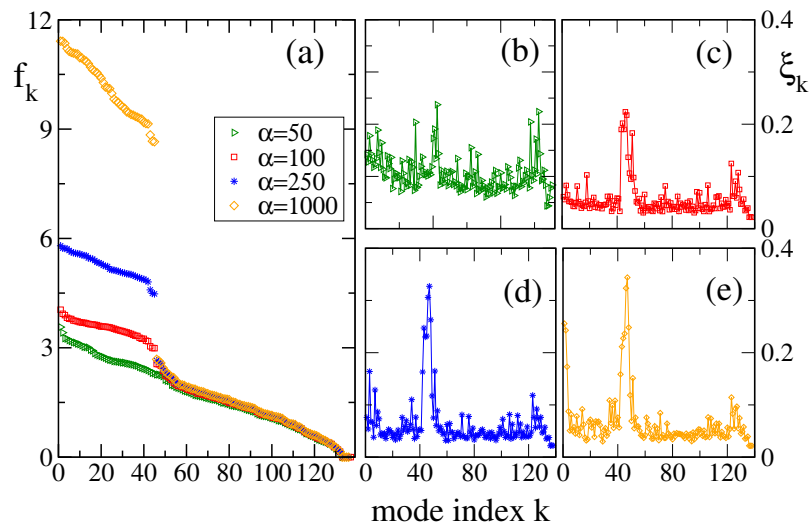


Figure 2. (Color Online) (a) Frequencies of the NMs, f_k . (b),(c),(d),(e) Inverse of the participation ratio for the corresponding eigenvectors for increasing value of the stiffness of the harmonic bonds. Triangles, squares, stars, and circles refer to $\alpha = 50, 100, 250$, and 1000 , respectively.

Furthermore, the formation of the gap is accompanied by a localization of the eigenvectors around the gap-facing band edges. In order to characterize the degree of localization of the k -th NM $\vec{e}_k(i)$ ($i = 1, 2, \dots, L$), we measured its *inverse participation ratio* [50],

$$\xi_k = \sum_{i=1}^L |\vec{e}_k(i)|^4 \quad (7)$$

where the eigenvectors are normalized to unity. For an eigenvector localized on a single site $\xi \simeq 1$, while for a completely delocalized state $\xi \simeq 1/L$. Therefore, the more the

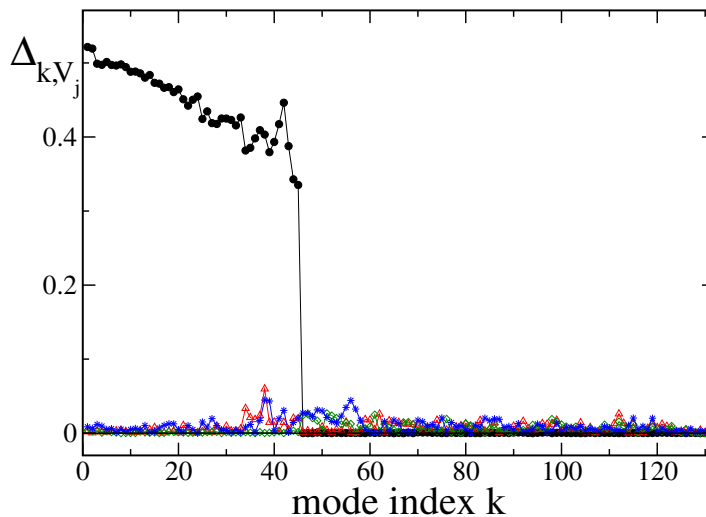


Figure 3. (Color online) Relative variations of the energetic contributions due to a perturbation of the NC along the direction of the k -th NM, as given by eq. (6), for $\alpha = 1000$. Circles, triangles, diamond and stars correspond to Δ_{k,V_H} , Δ_{k,V_A} , Δ_{k,V_D} , $\Delta_{k,V_{L,J}}$, respectively.

eigenvector is localized the larger is ξ . The inverse participation ratio is plotted in Fig. 2 (b-e) for different values of α . In particular, for $\alpha = 50$ all the eigenvectors are extended (see Fig. 2 (b)). However, by increasing α , the degree of localization of NMs in the lower optical band edge ($k = 43, 44, 45$) and of the first three NMs of the acoustic band edge ($k = 46, 47, 49$) increases (Fig. 2 (c-e)). A further increase in stiffness does not only lead to an enhancement of localization in the proximity of the gap, but also determines the localization of the first three optical eigenvectors ($k = 1, 2, 3$), see Fig. 2 (e). It is also interesting to observe that for increasing α the first and last three optical frequencies detach more and more from the band core (see again Fig. 2 (a)). In the following, we will fix $\alpha = 1000$.

We notice that the most localized modes of the optical band are localized at the three turns of the NC. More precisely, modes $k = 1, 45$ at the first turn (Fig. 4), NMs $k = 2, 44$ at the third turn and modes $k = 3, 43$ at the second one. The modes at both edges of the optical band are characterized by single or groups of neighbouring oscillators in opposition of phase, as shown in Fig. 4. Qualitatively, one may interpret them as impurity modes with the turns acting as structural defects [51]. Interestingly, for a toy model reproducing a single bent $2D$ chain with fixed curvature, Archilla *et al* [30] also reported a pair of localized modes lying at the band edge, with frequencies slightly detached from the band itself. Concerning the acoustic band-edge modes $k = 46, 47, 48$, only the y -component appears localized on the first and third β -strand B_9 , with the oscillators on the first and third strands in opposition of phase. Since these strands represent the core of the protein, we expect that excitation of these modes should cause large rearrangements in the structure, leading to protein unfolding.

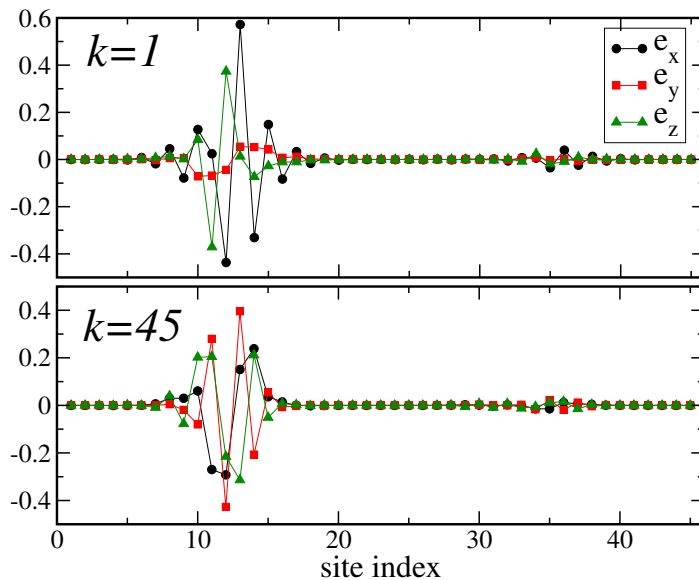


Figure 4. (Color Online) Cartesian components of the eigenvectors \vec{e}_1 (top) and \vec{e}_{45} (bottom) corresponding to the frequencies at the upper and lower edges of the optical band, respectively, for $\alpha = 1000$.

3. Emergence of discrete breathers

In this Section we show how DBs can be created by exciting the NC along the direction of certain NMs. In these simulations, we initialize the beads positions in the NC and assign the initial velocities proportional to the pattern of the selected NM. The amplitudes of the kinetic energy perturbation K_0 will be henceforth measured in temperature units $T = 2K_0/3L$, where a unitary Boltzmann constant is assumed.

As we shall show, the excitation of a normal mode provides an effective means of feeding energy to a discrete breather. However, due to specific selection rules matching spatial overlap between normal modes [64], a portion of the initial energy necessarily flows into a number of other modes. Such *background radiation* competes with the nonlinear localization process. This in turn, as we shall see in the following, accelerates the collapse of nonlinear modes. In order to analyze DB properties, it proves useful to get rid of background radiation through *surface damping* [23]. To this end, in the first part of the work we shall cool down the velocities of the beads at the chain terminals. More precisely, we integrate Hamilton's equations of motion while rescaling, at regular time intervals Δt , the momenta of the beads located at the chain terminals $i = 1, \dots, 4$ and $i = 43, \dots, 46$, that is

$$\vec{p}(i) \rightarrow \vec{p}'(i) = (1 - \gamma)\vec{p}(i) \quad \text{with} \quad \gamma \leq 1 \quad . \quad (8)$$

Unless otherwise specified, the cooling parameters are fixed to $\gamma = 0.001$ and $\Delta t = 0.02$. In section 3.1.1 a comparison between the dynamics with and without cooling is presented.

In order to visualize the energy localization along the chain highlighting the

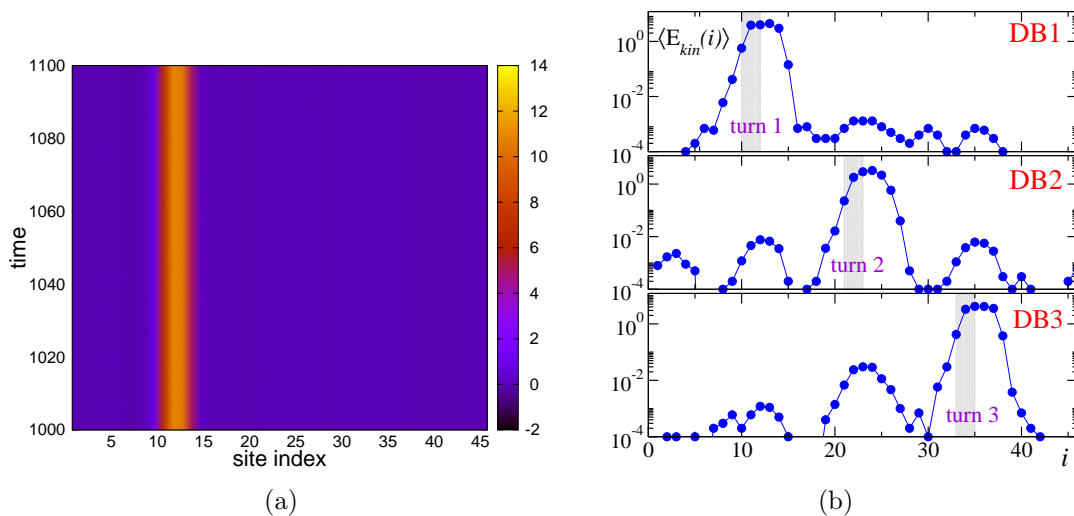


Figure 5. (Color Online) (a) Total energy difference per site $\Delta E_{tot}(i)$ with $i = 1, \dots, L$, as a function of time. for DB1 with an initial temperature $T = 0.63$. (b) Kinetic site energy $\langle E_{kin}(i) \rangle$ averaged over a time span of the order of 50 – 100 breather’s periods in order to smooth out fluctuations. From top to bottom DB1 with initial temperature $T = 0.63$, DB2 at $T = 0.42$ and DB3 at $T = 0.63$. Cooling parameters are $\gamma = 0.001$, $\Delta t = 0.02$ (a) and $\Delta t = 0.005$ (b). Grey regions mark the protein turns (see text).

emergence of a DB, we recorded the site kinetic energy $E_{kin}(i)$ and the total excitation energy per site $\Delta E_{tot}(i) = E_{kin}(i) + V(i) - V_{NC}(i)$, where $V(i)$ is the potential energy contribution which can be associated with the i -th bead (see Appendix A for the exact definition) and $V_{NC}(i)$ is the corresponding value in the NC. The presence of a DB is detected as a protracted concentration of energy on a limited number of sites.

Our first important observation is that a stable DB can be created by perturbing the NC along the direction of *each of the first 45 modes*, or along a linear combination of them. An example is reported in Fig. 5 (a) for the excitation of the lower optical-band edge mode. Remarkably, only three distinct breathers were observed to emerge despite the different directions of the employed perturbations. They are located close to the three turns and we thus denote them as DB1, DB2, and DB3, after the index of the corresponding turn (Fig. 5 (b)).

A peculiarity of such localized modes is that they feature patterns that are not simply localized over a few adjacent sites. Rather, they display non-negligible components localized elsewhere in the chain. This can be appreciated by looking to the average site kinetic energy reported in Fig. 5 (b) for the three breathers. The largest contribution to the DB total energy comes indeed from the few sites located at the corresponding turn. However, energy components two-orders of magnitude smaller can be found over the other turns too. The origin of this peculiar localization patterns can be found in the three-dimensional structure of the protein, and it is induced by the requirement of momentum conservation. In other words, the special built-in momentum-

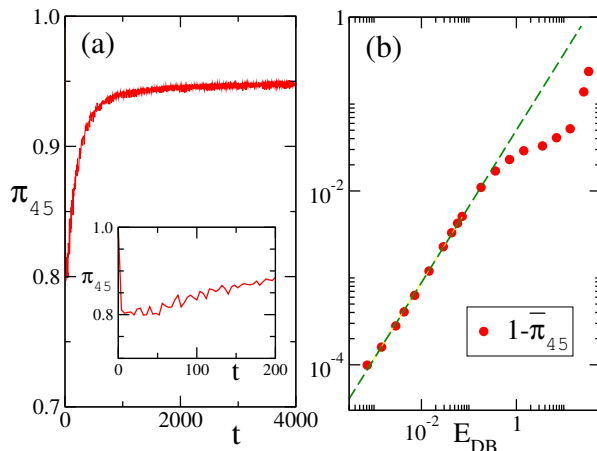


Figure 6. (Color online) DB obtained as a continuation of NM $k = 45$. (a) Time evolution of the projection π_{45} for $T = 0.21$. The inset shows a close-up of the short-time dynamics. (b) $1 - \bar{\pi}_{45}$ as a function of the total energy E_{DB} . The dashed line is a power law of the type $1 - \bar{\pi}_{45} \propto E_{DB}^\eta$ with $\eta \approx 0.88$.

conservation properties of NM patterns are reproduced by DBs. As a matter of fact, it turns out that a mode that is localized at a few sites conserves its momentum by fractioning an equal and opposite amount of momentum among few other locations, instead of spreading it over the whole structure. The interesting question arises whether this is a generic feature of NMs in proteins or it is rather the expression of the peculiar native fold considered here.

The three DBs can be considered as nonlinear continuations of three corresponding NMs, that are localized at the same turns and whose vibration patterns can be considered as precursors of the DB displacement fields. This is confirmed by looking at the normalized projections π_k of the breathers' velocity fields on the corresponding modes, defined as:

$$\pi_k = \left\langle \sum_{i=1}^L \frac{\vec{p}(i)}{\sqrt{2K}} \cdot \vec{e}_k(i) \right\rangle_t \quad (9)$$

where the angular brackets denote the average over a window of w time units ($w = 4.0$ in the following). Fig. 6 (a) shows that, for DBs originating from NM 45, after an initial transient π_{45} shows a stable trend with very small residual oscillations around the mean value $\bar{\pi}_{45}$ evaluated in the last stage of the simulation ($3000 \leq \text{time} \leq 4000$). The projections on the other modes (not shown in the figure) are smaller than 0.015. In Fig. 6 (b) we plot $1 - \bar{\pi}_{45}$ as a function of the DB total energy, $E_{DB} = K + V - V_{NC}$, measured in the last stage. The figure shows that $1 - \bar{\pi}_{45}$ vanishes when the energy is decreased following a nearly linear trend.

These results confirm and generalize what reported in the context of the Nonlinear Network Model (NNM), where gap-less breathers were shown to arise as continuations of edge NMs [15]. Also in the framework of the NNM, few special regions were shown to act as energy-accumulating centres upon generic excitation of the system, exactly as

we observed here [23].

Perturbations along all the optical modes of amplitude $T = 0.63$ resulted in the excitation of DB1 or DB3, while DB2 was observed only in a few cases. The reason why DB2 seems somehow more difficult to excite is likely to depend upon the peculiar structural neighborhood of the second turn. This region lies deeper inside the core of the protein, where beads are more constrained, thus hindering the DB oscillations (see also the cartoon showing DB patterns in Fig. 8).

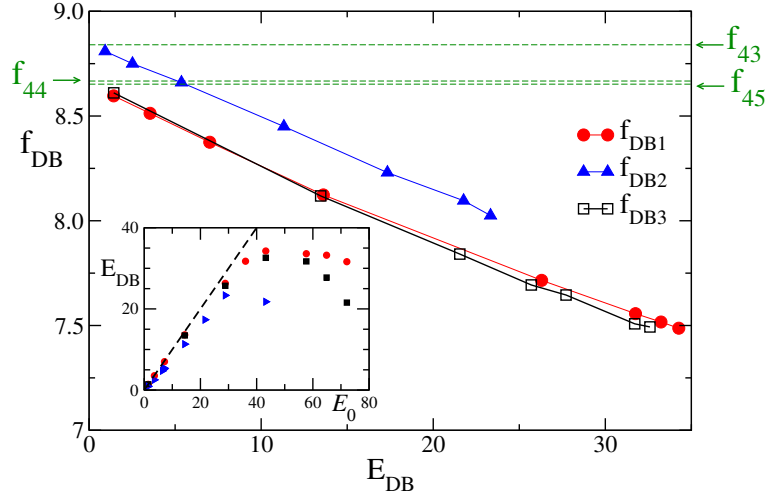


Figure 7. (Color online) DBs originating from $k = 45$ (DB1), $k = 43$ (DB2) and $k = 44$ (DB3). Frequencies of DBs as a function of their total energy E_{DB} . The horizontal dashed lines flag the frequencies of the corresponding NMs. The inset displays E_{DB} as a function of the initial energy $E_0 = K_0 - V_{NC}$ for the three DBs: circles, triangles, squares refer to DB1, DB2, DB3, respectively. The dashed line marks the *full-efficiency* regime $E_{DB} = E_0$.

The DB frequencies f_{DB1} , f_{DB2} and f_{DB3} are computed from the power spectrum of the displacements of the most energetic bead within each DB. Typical DB spectra feature a main peak and minor (several orders of magnitude smaller) peaks signalling the residual excitation of few normal modes. The measured frequencies are shown in Fig. 7 as functions of the DB total energy E_{DB} , all three DBs exhibit an almost linear decrease characterized by the same dispersion relation $f_{DB}(E_{DB}) = f_k(1 - E_{DB}/\varepsilon)$, where f_k is the frequency of the NM from which the DB originates and $\varepsilon \approx 250$. We notice that ε could be in principle calculated through Lindstedt-Poincaré perturbation theory as done, for example, in Ref. [15].

The decrease of the DB frequency with the energy E_{DB} suggests that the relevant nonlinearity is of the *soft* type [18]. This explains why the presence of a gap is necessary for the formation of localized nonlinear modes. Indeed, we were unable to excite DBs in cases where the spectrum is gap-less.

The frequencies f_{DB1} and f_{DB3} originate from the bottom of the optical band ($f_{44} \approx f_{45}$) and enter the gap for arbitrary small energies. On the contrary, f_{DB2}

lies between f_{43} and f_{44} for small energies, staying manifestly non-resonant with the neighbouring optical modes. This behaviour is reminiscent of intra-band DBs predicted by Kopidakis and Aubry in nonlinear disordered chains [52, 53] and found analytically in nonlinear network models of proteins [15]. For larger energies, the frequency decreases further and also these DBs eventually enter the gap.

It is instructive to consider whether a given DB can be created with arbitrary energy by exciting a given normal mode. The inset in Fig. 7 shows the relation between the initial total energy $E_0 = K_0 - V_{NC}$ and the energy that is found stored in the DB. The ratio of the two values can be interpreted as an estimate of *transfer efficiency*, i. e. the fraction of the initial excitation energy channeled into the DB and consequently pinned down at a very specific location. Remarkably, we see that all the three DBs are characterized by a nearly unitary efficiency, up to a point where the curve saturates and then starts bending down. The transfer of energy from the NM to the DB is nearly optimal up to initial energies of the order $E_0 = K_0 - V_{NC} \approx 30$. This indicates the existence of a sort of maximal "DB capacity" – if the NM is feed with larger energies, the excess energy cannot be further injected in a localized mode and it is necessarily spread across the whole structure.

Finally, no DB could be excited by perturbing the structure along acoustic NMs. This is most likely a consequence of the soft nonlinearity. Moreover, we were also unable to excite DBs through arbitrary localized perturbations of the NC. Indeed, initial conditions of the latter type have non-zero components over many NMs, including the acoustic ones.

3.1. DBs originating from the lower optical-band edge

In this section we shall present a more detailed analysis of the properties of DB1 originating from the bottom optical mode $k = 45$. This breather is localized on the first turn, from site 10 to site 14, as it is shown in Fig. 5. The energy redistribution dynamics within the DB can be appreciated from Fig. 9 (a). In particular, it is clear that the two site pairs (12,13) and (11,14) exhibit approximately phase-locked oscillations, while they are anti-phase locked among them. This is another illustration of the fact that the DB exchanges little or no energy with the surrounding.

It is instructive to analyse the different contributions to the total energies when the DB is present, in order to quantify to what extent the different degrees of freedom participate to the breather dynamics. As it can be seen from Fig. 9 (b), at one of the most energetic sites, $i = 12$, the DB vibration involves essentially the backbone bonds ($\approx 84 - 86\%$) with a small contribution coming from the angular terms ($\approx 13 - 15\%$), while the dihedral and Lennard-Jones contributions are negligible. The observed ratios between the different energetic contributions do not change by varying the initial energy. We observe the same behaviour for all the sites in the interval (11 – 13).

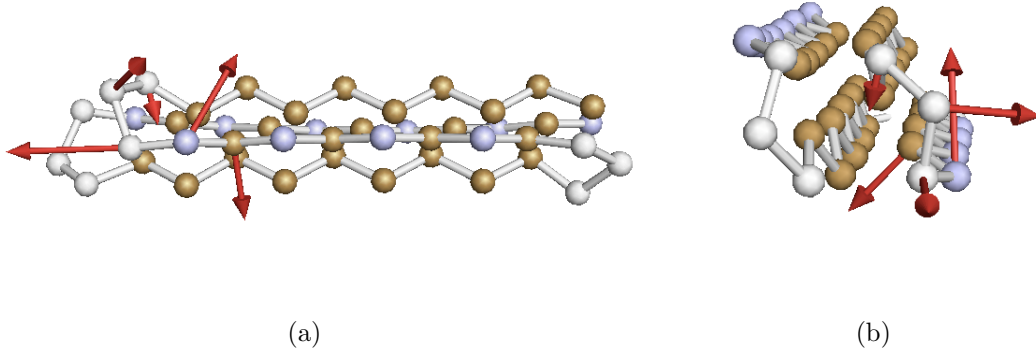


Figure 8. (Color online) Displacement field of DB1. Side (a) and front (b) views (only displacements larger than 1.0 have been shown as arrows). The initial condition corresponds to $T = 0.63$.

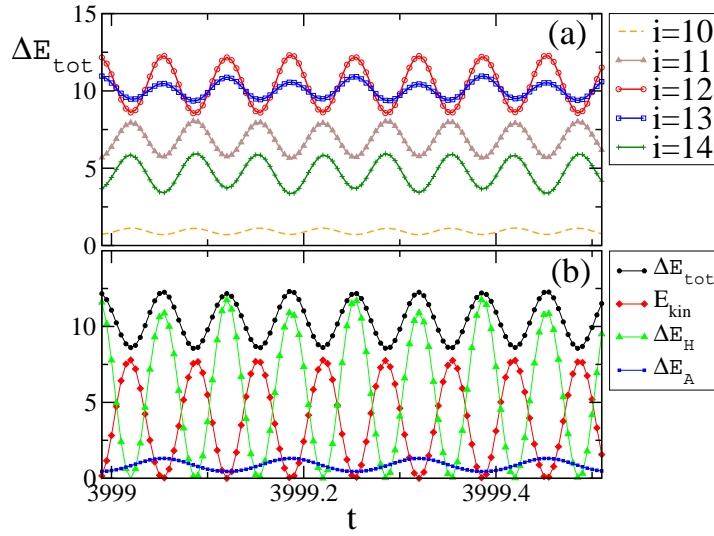


Figure 9. (Color online) (a) Total site energies for DB1 and (b) the different energy contributions at site $i = 12$ versus time ($\Delta E_j = V_j - V_{NC}(j)$ where $j = H, A$, the dihedral and Lennard-Jones contributions being negligible). Parameters are: $T = 0.63$, $\gamma = 0.001$, $\Delta t = 0.005$.

A closer inspection of Fig. 9 (b) shows that the harmonic bond component oscillates at frequencies $2f_{DB}$ but also has a sizeable component at f_{DB} . This is due to the soft nonlinearity which is known to induce a DC component in the displacement patterns of localized modes [54, 19]. To understand this in a simple way, let us consider two bond lengths along the backbone at site n , $r_1 \equiv r_{n-1,n}$ and $r_2 \equiv r_{n,n+1}$. We may write their evolution as an oscillating part plus a static distortion of the bond lengths,

$$\begin{aligned} r_1(t) &= A_1 \sin(\omega t) + \langle r_1 \rangle \\ r_2(t) &= A_2 \sin(\omega t) + \langle r_2 \rangle \end{aligned}$$

where $\omega = 2\pi f_{DB}$ and the angular brackets represent a time average. Using the definition reported in Appendix A, it can be shown that the contribution of the two bonds to the local harmonic energy is

$$\begin{aligned}
 V_H(n) \propto & \frac{(A_1^2 + A_2^2)}{2} \sin^2(\omega t) \\
 & + [A_1(\langle r_1 \rangle - r_0) + A_2(\langle r_2 \rangle - r_0)] \sin(\omega t) \\
 & + \frac{(\langle r_1 \rangle - r_0)^2 + (\langle r_2 \rangle - r_0)^2}{2}
 \end{aligned} \tag{10}$$

Thus, the presence of a component at frequency ω implies that $\langle r_1 \rangle$ and/or $\langle r_2 \rangle$ must be different from their equilibrium value r_0 . Accordingly, we conclude that the emergence of a DB also causes a stable structural distortion of the protein. Given that $A_1 \approx A_2 \approx 0.1$ (see again Fig. 9), also tiny differences $\langle r_i \rangle - r_0 \approx 10^{-3}$, as we recorded in our simulations, are able to affect the local bond energies.

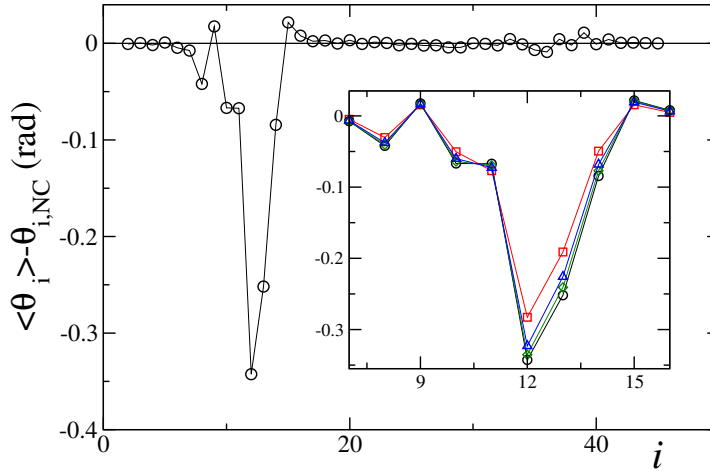


Figure 10. (Color online) Difference between the average values of the bond-bond angles θ_i when the DB1 is present and the corresponding equilibrium values (in the NC), $\theta_{i,NC}$, when the total energy of DB1 is $E_{DB} = 34.6$. The inset shows a close-up of the kink region for increasing energies: (red) squares, (blue) triangles, (green) diamonds, (black) circles refer to $E_{DB} = 26.3, 31.68, 33.61, 34.6$, respectively.

Much more prominent is the distortion effect caused by the soft-nonlinearity in the angular degrees of freedom. In particular, Fig. 10 reveals that the breather is also characterized by a kink-shaped angular distortion. The kink's amplitude increases with the total energy stored in the breather (see the inset in Fig. 10).

3.1.1. DB collapse and the effect of cooling In the case where no cooling is applied ($\gamma = 0$) the DBs have a finite lifetime. To illustrate this, in Fig. 11 (a) we report the time evolution of the projection π_{45} of the DB1, obtained as a continuation of the lower optical-band edge mode ($k = 45$). The sudden drop of π_{45} signals the collapse of the excitation, accompanied by a rapid redistribution of energy over all the normal modes (equipartition). The typical collapse time increases upon decreasing the initial energy

(compare the three curves in Fig. 11 (a)). This is similar to what demonstrated for one-dimensional chains where the time to equipartition scales as an inverse power of the energy density [55, 56].

The effect of the collapse of a DB on the protein structure can be appreciated by considering the Kabsch distance δ_K , which is a commonly used measure of the structural distance between two protein configurations [57]. In particular, Fig. 11 (b) shows how the distance δ_K of the protein structure from the NC evolves in time in the presence of a discrete breather of type DB1. As long as the DB is present, δ_K fluctuates around a relatively small value ($\delta_K \simeq 0.1$), meaning that the protein structure does not deviate appreciably from the NC. In fact, the static distortion effect illustrated above only concerns a small region of the fold. On the other hand, when the DB collapses, δ_K starts to fluctuate wildly around a substantially larger value ($\delta_K \approx 0.35$), thus signaling the occurrence of important conformational rearrangements.

The DB lifetime gets substantially increased by removing the background vibrations through cooling. Fig. 11 (c) clearly illustrates how dissipation renders the DB stable by quickly eliminating background radiation. The stabilizing role of the boundary cooling method is well documented [58, 59, 23] and our results confirm that it can be used conveniently also for such a complex structure.

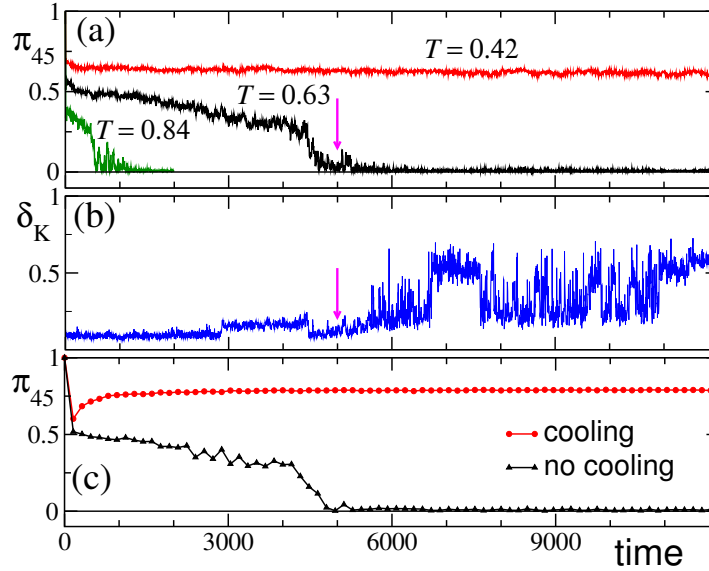


Figure 11. (Color online) (a) Projection of the DB1 velocity field on the $k = 45$ NM, π_{45} , as a function of time for increasing values of the initial energy. From the top to the bottom curve, $T = 0.42, 0.63, 0.84$ (non-dissipative dynamics). (b) Kabsch distance δ_K for $T = 0.63$ (non-dissipative dynamics). The vertical arrows mark the time at which the DB collapses. (c) Comparison of π_{45} for dissipative (upper red line), and non-dissipative (lower black line) dynamics for $T = 0.63$.

3.2. Excitation of optical band-edge NMs: long-range energy transfer

The excitation of NMs at the upper edge of the spectrum gives rise to quite peculiar phenomena. As a first example, Figs. 12 depict the emergence of a DB obtained by exciting the first two highest-frequency NMs, i.e. \vec{e}_1 , which is localized at sites 10 – 12 and \vec{e}_2 , which is localized at sites 34 – 36. In the first stage, the energy quickly spreads and remains confined in the vicinity of the perturbed location. After some time, a DB self-localizes, harvesting energy from the background and pinning it in the same region. The DBs obtained are again DB1 and DB3. This is reasonable in view of the similar spatial structure of \vec{e}_1 , \vec{e}_2 and DB1, DB3, respectively (see again Fig.4). Moreover, we found that the frequencies of DBs originating from \vec{e}_1 lie on the same frequency-energy curve as the breather originating from normal mode 45, shown in Fig. 7.

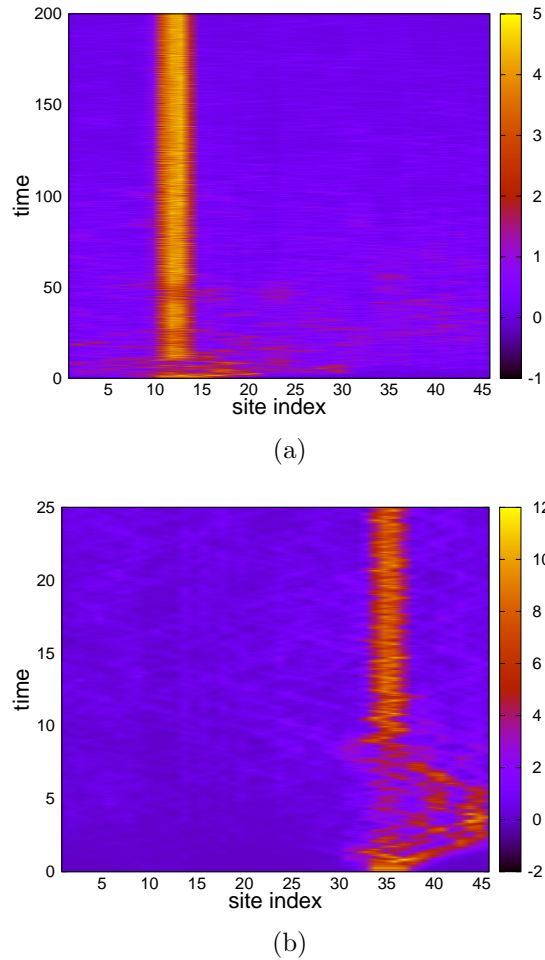


Figure 12. (Color online) Time evolution of total site energies starting from excitation of the upper band-edge optical modes: (a) Emergence of DB1 from \vec{e}_1 , $T = 0.63$ and (b) of DB3 from \vec{e}_2 , $T = 0.84$.

Remarkably, we have also observed that the excitation of an edge mode may result

in a *long-range energy transfer* event. An illustration of this phenomenon is given in Fig. 13(a), for the excitation of the third highest-frequency NM. The NM \vec{e}_3 is localized at sites 22 – 27. Immediately after the perturbation, the DB appears localized in the same region, but seems to collapse rapidly afterwards, spreading its energy evenly across the structure. However, after a considerable time span, another DB emerges at a different location, namely at sites 11 – 13. This is the region where the lower optical-band edge mode ($k = 45$) is localized. A substantial part of the initial energy has been transferred and pinned down irreversibly at the other end of the structure, covering the distance from a turn to the following one (see again the cartoon depicting the protein structure).

Such energy transfer phenomenon can be rationalized by analyzing the projections of the DB velocity field on the NMs during the time evolution of the perturbation. From Fig. 13 (b) one can clearly see that the initially excited mode is quickly emptied of its initial energy, which gradually flows into other two modes. As it shows, asymptotically the two target modes almost describe the entirety ($\pi_{44} + \pi_{45} \approx 1$) of the DB, which is in fact localized at the turn opposite to the excited one, where the two target NMs are also localized. The reverse process is forbidden since the DB frequency is no longer resonating with the original mode. We remark that this phenomenon, although evocative of resonant energy transfer among few selected normal modes in proteins, is a one-way transfer, as the DB will retain the transferred energy for times comparable to its lifetime [60, 61].

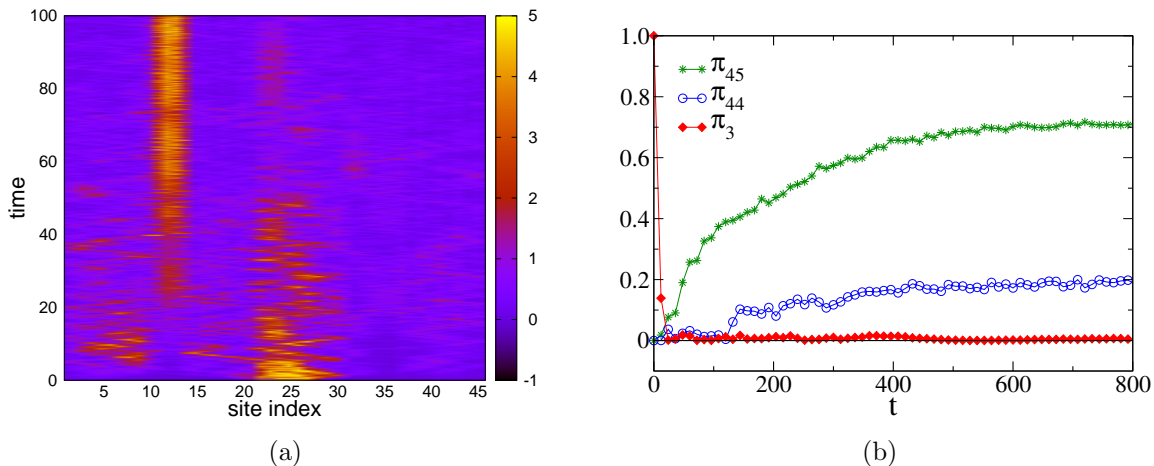


Figure 13. (Color online) Long-range energy transfer starting from \vec{e}_3 at $T = 0.63$. (a) Time-evolution of total site energies; (b) projections of the DB velocity field on three NMs as functions of the time.

3.3. Excitation of deep-band NMs

NMs in the core of the optical band are generally characterized by a low level of localization, as one can see in Fig. 2 (b-e). As a result, when one of such modes is

excited, we observe a complex localization pattern, that alternates site-hopping and energy-pinning stages to phases where the energy is more evenly distributed. After a certain time, a stable DB emerges, focusing the energy at one of the turns. A typical realization of this scenario is illustrated in Fig. 14(a) for the excitation of the fifth highest-frequency mode.

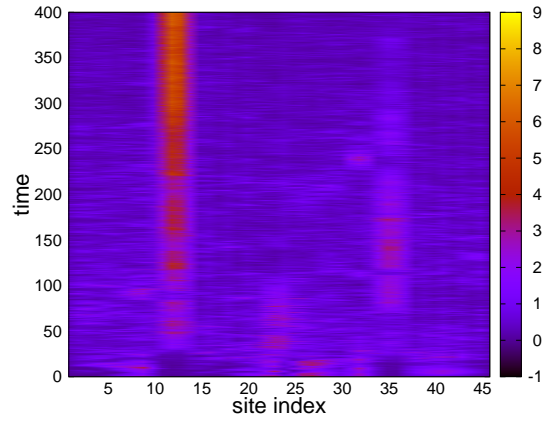
A different phenomenology is observed when we excite a mode lying deeper within the band. It may occur that the excitation energy remains trapped in two DBs localized on two different turns, realizing a state which is reminiscent of multibreather states observed in non-linear disordered systems [52, 53]. A realization of this phenomenon for NM 33 is reported in Fig. 14 (b). In particular, we notice that starting from NM 33 and changing the initial energy we can get different solutions. For example, for $T = 0.21$ we obtain a solution localized on the first and second turn, while the multibreather localizes on the first and third ones for $T = 0.63$.

A very peculiar localized solution develops through the excitation of normal mode $k = 36$, whose pattern is localized in the protein's tail. As it is shown in Fig. 14 (c), the energy remains almost entirely confined to the edge sites 44 – 46, with smaller, but non-negligible, amounts of energy also involving the turns Fig. 15 (a). We term such excitations *boundary breathers* (BB). As in the case of DB1, DB2 and DB3, the frequency of oscillation of the BB also lies in the gap ($f_{BB} = 7.739$ for $E_{DB} = 34.75$). At variance with DB1, DB2, DB3, the energy of BBs has not only harmonic and angular contributions but also a sizeable Lennard-Jones one, resulting from a non-negligible interaction between the first and last beads, as well as the second turn region of the chain which are relatively close in the NC. We note that nonlinear surface states of different kinds are known and studied in many contexts [19, 62].

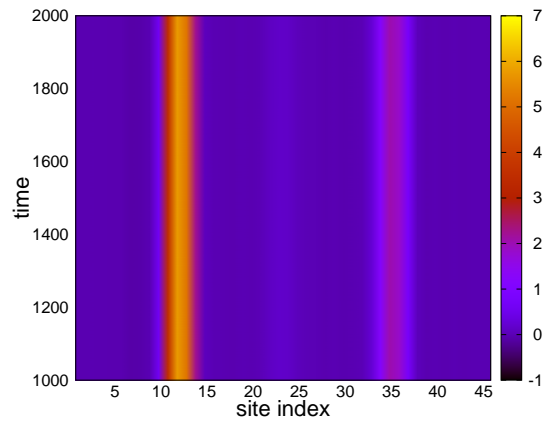
Eventually, the BBs hop to one of the three breathers described above. Fig. 16 illustrates an example of this process, where the BB transfers its energy to DB3, as confirmed by the time evolution of the normal-mode projections shown in Fig. 15 (b). Asymptotically, we see that the main projection is π_{36} , while at $t \approx 2.75 \times 10^3$ an abrupt transition occurs and the leading projection becomes π_{44} , signalling the energy transfer to DB3 (corresponding to NM $k = 44$) localized at the third turn.

While at high energies, *i.e.* $T = 0.84, 1.05$, the lifetime of BBs before a transition to DB3 takes place is short, at lower energies we observe the formation of a transient multibreather-like state with a progressive transfer of energy from BB to DB3. One of such examples is depicted in Fig. 16. Decreasing the excitation energy further, BBs are no longer observable.

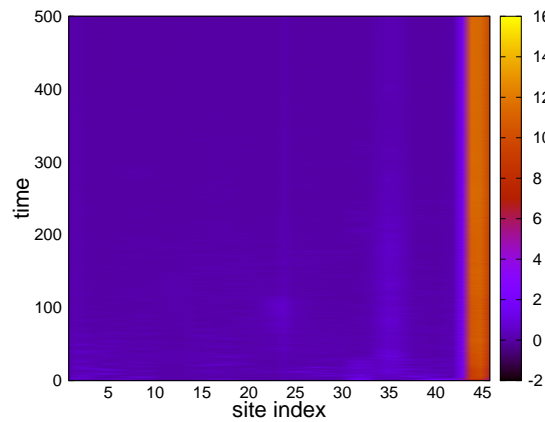
We note that the end of the protein can be considered as a defect/discontinuity in the chain, since it is a free end that interrupts the chain itself. Therefore, BBs can be considered as akin to localized modes emerging in other contexts close to point defects. Furthermore, we were unable to excite stable BBs localized on the first beads of the sequence, despite NMs with significative components on that terminal do exist. A possible explanation of this apparently contradictory result is the fact that the first strand is part of the protein core. Therefore, it is a much more rigid structure with



(a)



(b)



(c)

Figure 14. (Color online) Evolution of total site energies starting from excitation of the deep-band optical modes: (a) Emergence of DB1 from \vec{e}_5 , $T = 0.63$ and (b) multibreather solution localized on the first and third turn starting from \vec{e}_{33} at $T = 0.63$; (c) Boundary Breather (BB) following the excitation of mode \vec{e}_{36} , $T = 0.84$ (non-dissipative dynamics).

respect to the last strand, which instead is exposed to the solvent and can oscillate more freely.

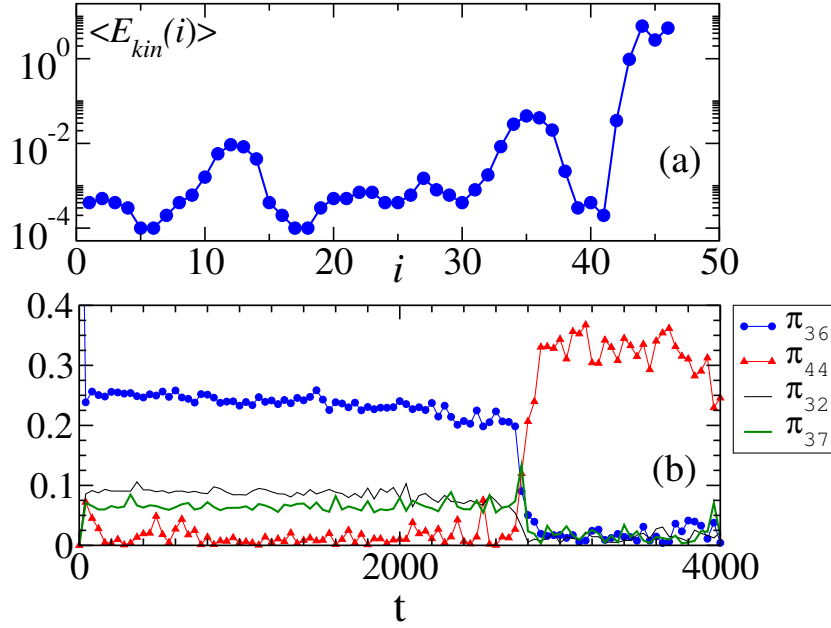


Figure 15. (Color online) Emergence of a Boundary Breather (BB) following the excitation of mode $k = 36$ with $T = 0.63$. (a) time-averaged site kinetic energies (the cooling is applied to the first 4 beads); (b) projections of the DB normalized velocity field on the NMs as a function of time (non-dissipative dynamics).

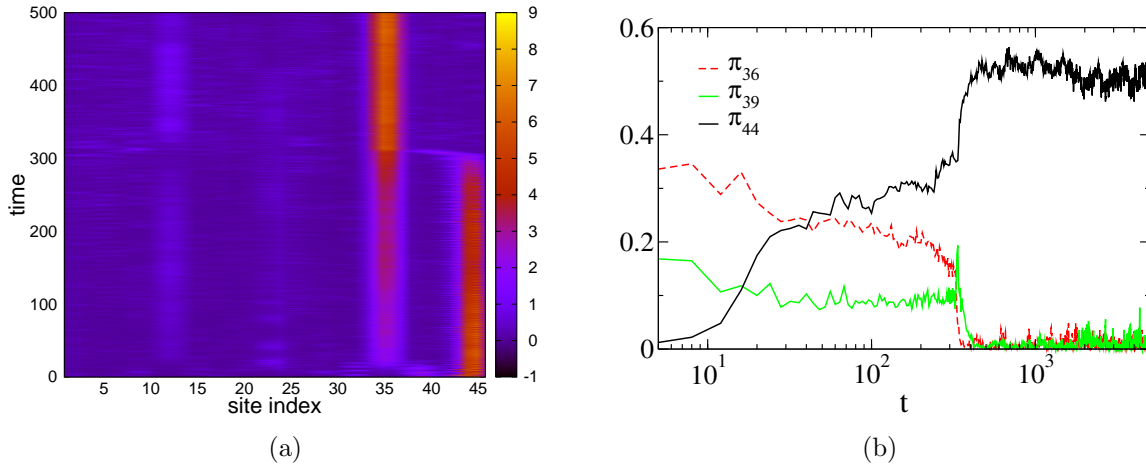


Figure 16. (Color online) Transient multibreather-like mode, localized on the protein boundary and on the third turn, obtained following the excitation of the $k = 36$ NM at $T = 0.42$ (non-dissipative dynamics). (a) Space-time plot of the total site energies. (b) Normalized projections of the DB velocity field on the NMs as a function of the time.

4. Conclusions

In this paper we have reported the existence of discrete breathers in an off-lattice model of proteins with realistic interaction potentials and three-code amino-acid sequence. To our knowledge, this is the first time that this class of peculiar vibrational modes are found in such a complex and heterogeneous dynamical system. In particular, we have shown that, due to the softness of the leading nonlinearity, a necessary condition for DB existence is that the linear spectrum exhibits a gap (at least one), as it is indeed the case in all proteins.

For the particular structure analyzed in this work, we have identified three families of DBs, each one localized on a different turn of the native fold. The largest fraction of the energy of a discrete breather typically resides on a few sites and involves essentially harmonic and angular degrees of freedom, while dihedral and Lennard-Jones interactions between distant sites are practically not excited.

We have obtained discrete breathers as continuations of the lower optical band-edge normal modes. Quite generically, however, we have shown that members of the three different breather families can be excited by feeding energy to *any* of the normal modes lying in the optical band. Remarkably, the excitation of a DB obtained by feeding energy to a given normal mode is an extremely *efficient* process. This means that there is an extended range of initial energies that can be fed to the system and immediately channeled almost entirely into a breather, which is permanently localized at a very specific location.

Our results prove that DBs have a stabilizing effect on the protein. In fact, a broad class of perturbations of the native fold result in the formation of a DB, that is, a stable and highly localized vibration, while on the other hand long-range contacts are almost devoid of energy. This enhances the structural stability of the protein. To this regard, it would be interesting to connect the structure-dynamics relation underlying DB formation to the well-conserved patterns of nucleation sites along folding pathways [63].

We also discovered peculiar DB-assisted long-range energy transfer phenomena, whereby energy is channeled to a distant region of the structure away from the excitation site. At variance with ordinary energy exchange between resonant normal modes [64], this is a one-way process, meaning that the transferred energy is never released back to the starting location. In particular, this effect may be of importance in the functioning of allosteric proteins [65, 6, 66] and surely deserves further investigation.

Our work has highlighted nontrivial correlations between structural and dynamical features of protein folds. In a simple β -barrel, as the one here considered, localization occurs on loops. Concerning more complex structures, our results raise the important question whether more complex structural selection rules exist driving nonlinear energy localization and long-range targeted transfer.

Acknowledgments

We acknowledge useful discussions with S. Flach, R. Livi and L. Schimansky-Geier. Thanks are due to S. Allaccia and A. Scarpa for inspiring the style and presentation of the paper. AT gratefully acknowledges the financial support of Aarhus Universitet Forskning Fonden (AUFF) during his stay at Aarhus University. AI is partially supported by Lundbeck Fonden. This work is part of the CNR-RSTL project N. 827 *Dinamiche cooperative in strutture quasi uni-dimensionali*. Finally, we thank the Danish Centre for Scientific Computing for providing us with computational resources.

Appendix A: Single Site Energy

Since each potential energy term represents a many-body interaction, we have estimated the single-site potential energies $V(i)$ by equally redistributing the energy to each site involved in the different terms and then by summing up all this contributions.

In particular, the harmonic term is a two body potential involving nearby sites, therefore the contribution is estimated as follows

$$V_H(i) = \begin{cases} \sum_{k=i}^{i+1} V_H(r_{k-1,k})/2 & \text{for } i = 2, L-1 \\ V_H(r_{1,2})/2 & \text{for } i = 1 \\ V_H(r_{L-1,L})/2 & \text{for } i = L \end{cases} .$$

The angular term is a three body interaction involving three consecutive sites, and therefore

$$V_A(i) = \begin{cases} \sum_{k=i-1}^{i+1} V_A(\theta_k)/3 & \text{for } i = 3, L-2 \\ V_A(\theta_2)/3 & \text{for } i = 1 \\ \sum_{k=2}^3 V_A(\theta_k)/3 & \text{for } i = 2 \\ \sum_{k=L-2}^{L-1} V_A(\theta_k)/3 & \text{for } i = L-1 \\ V_A(\theta_{L-1})/3 & \text{for } i = L \end{cases} .$$

The dihedral angle φ is the angle between two nearby planes each containing three consecutive sites, the corresponding potential term is therefore a four-body term, and the single site contribution can be evaluated as follows

$$V_D(i) = \begin{cases} \sum_{k=i-2}^{i+1} V_D(\varphi_k, \theta_k, \theta_{k+1})/4 & \text{for } i = 4, L-3 \\ V_D(\varphi_2, \theta_2, \theta_3)/4 & \text{for } i = 1 \\ \sum_{k=2}^3 V_D(\varphi_k, \theta_k, \theta_{k+1})/4 & \text{for } i = 2 \\ \sum_{k=2}^4 V_D(\varphi_k, \theta_k, \theta_{k+1})/4 & \text{for } i = 3 \\ \sum_{k=L-4}^{L-2} V_D(\varphi_k, \theta_k, \theta_{k+1})/4 & \text{for } i = L-2 \\ \sum_{k=L-3}^{L-2} V_D(\varphi_k, \theta_k, \theta_{k+1})/4 & \text{for } i = L-1 \\ V_D(\varphi_{L-2}, \theta_{L-2}, \theta_{L-1})/4 & \text{for } i = L \end{cases} .$$

The Lennard-Jones term is a two-body interaction involving sites separated by more than two bonds along the chain

$$V_{LJ}(i) = \sum_j V_{LJ}(r_{ij})/2 \text{ for } |i - j| > 2 \quad .$$

The total site potential energies read

$$V(i) = V_H(i) + V_A(i) + V_D(i) + V_{LJ}(i).$$

References

- [1] Creighton T E 2002 *Proteins: Structures and Molecular Properties* (New York: W.H. Freeman & Co)
- [2] Yang L and Bahar I 2005 *Structure* **13** 893–904
- [3] Bahar I, Erman B, Jernigan R L, Atilgan A R and Covell D G 1999 *J. Mol. Biol.* **285** 1023–1037
- [4] Eisenmesser E Z, Bosco D A, Akke M and Kern D 2002 *Science* **295** 1520–1523
- [5] Kondo J, Urzhumtsev A and Westhof E 2006 *Nucl. Ac. Res.* **34** 676–685
- [6] del Sol A, Tsai C J, Ma B Y and Nussinov R 2009 *Structure* **17** 1042–1050
- [7] Delarue M and Sanejouand Y H 2002 *J. Mol. Biol.* **320** 1011–1024
- [8] Zheng W and Brooks B R 2005 *Biophys. J.* **88** 3109–3117
- [9] Elezgaray J, Marcou G and Sanejouand Y H 2002 *Phys. Rev. E* **66** 31908–31915
- [10] Brooks B R and Karplus M 1985 *Proc. Natl. Acad. Sci. USA* **82** 4995–4999
- [11] Marques O and Sanejouand Y H 1995 *Proteins* **23** 557–560
- [12] Murray J, Hu Q, Navenot J and Peiper S 2002 *Biochem. Biophys. Res. Commun.* **292** 449–455
- [13] Manley M E, Sievers A J, Lynn J W, Kiselev S A, Agladze N I, Chen Y, Llobet A and Alatas A 2009 *Phys. Rev. B* **79** 134304
- [14] Bahar I, Atilgan A R, Demirel M C and Erman B 1998 *Physical Review Letters* **80**
- [15] Piazza F and Sanejouand Y H 2008 *Phys. Biol* **5** 026001
- [16] Sacquin-Mora S, Laforet E and Lavery R 2007 *Proteins* **67** 350–359
- [17] Sievers A J and Takeno S 1988 *Physical Review Letters* **61**
- [18] Flach S and Willis C R 1998 *Physics Reports* **295** 181–264
- [19] Flach S and Gorbach A V 2008 *Physics Reports* **467** 1–116
- [20] Trias E, Mazo J J and Orlando T P 2000 *Physical Review Letters* **84**
- [21] Binder P, Abramov D, Ustinov A V, Flach S and Zolotaryuk Y 2000 *Physical Review Letters* **84**
- [22] Sato M and Sievers A 2009 *Journal of biological physics* **35** 57–72
- [23] Juanico B, Sanejouand Y H, Piazza F and De Los Rios P 2007 *Phys. Rev. Lett.* **99** 238104
- [24] Piazza F and Sanejouand Y H 2009 *Physical Biology* **6** 046014
- [25] Piazza F and Sanejouand Y H 2009 *Europhysics Letters* **88** 68001
- [26] Piazza F and Sanejouand Y H 2010 *to appear in Discrete and Continuous Dynamical Systems, Series S*
- [27] Sitnitsky A E 2006 *Physica A: Statistical and Theoretical Physics* **371** 481–491
- [28] Agarwal P K 2005 *Journal of the American Chemical Society* **127** 15248–15256
- [29] Salerno M and Kivshar Y S 1994 *Physics Letters A* **193** 263–266
- [30] Archilla J F R, Gaididei Y B, Christiansen P L and Cuevas J 2002 *Journal of Physics A* **35** 8885–8902
- [31] Sánchez-Rey B, Archilla J F R, Palmero F and Romero F R 2002 *Physical Review E* **66** 017601
- [32] Honeycutt J D and Thirumalai D 1990 *Proceedings of the National Academy of Sciences of the United States of America* **87** 3526–3529
- [33] Berry R S, Elmaci N, Rose J P and Vekhter B 1997 *Proceedings of the National Academy of Sciences of the United States of America* **94** 9520–9524

- [34] Guo Z and Thirumalai D 1995 *Biopolymers* **36** 83–102
- [35] Guo Z and Brooks C L 1997 *Biopolymers* **42** 745–757
- [36] Veitshans T, Klimov D and Thirumalai D 1997 *Folding and Design* **2** 1–22
- [37] Evans D A and Wales D J 2003 *The Journal of Chemical Physics* **118** 3891–3897
- [38] Kim J, Straub J E and Keyes T 2006 *Physical Review Letters* **97** 050601
- [39] Kim J M and Keyes T 2007 *Journal of Physical Chemistry B* 2647
- [40] Li F Y, Yuan J M and Mou C Y 2001 *Physical Review E* **63** 021905
- [41] Lacks D J 2005 *Biophysical journal* **88** 3494–3501
- [42] Imparato A, Luccioli S and Torcini A 2007 *Physical Review Letters* **99** 168101
- [43] Luccioli S, Imparato A and Torcini A 2008 *Physical Review E* **78** 031907
- [44] Imparato A, Luccioli S and Torcini A 2010 *Prog. Theor. Phys. Supplement* **184** 339–350
- [45] Luccioli S, Imparato A, Mitternacht S, Irbäck A and Torcini A 2010 *Physical Review E* **81** 010902
- [46] Blondel A and Karplus M 1996 *Journal of Computational Chemistry* **17** 1132–1141
- [47] Rampioni A 2005 *Caratterizzazione del panorama energetico di piccoli peptidi al variare della loro lunghezza* Ph.D. thesis University of Florence Italy
- [48] Atela P and McLachlan R I 1992 *Nonlinearity* **5** 541
- [49] Wales D J 2003 *Energy Landscapes* (Cambridge: Cambridge University Press)
- [50] Aoki H 1983 *Journal of Physics C: Solid State Physics* **16** L205
- [51] Forinash K, Peyrard M and Malomed B 1994 *Phys. Rev. E* **49** 3400–3411
- [52] Kopidakis G and Aubry S 2000 *Physica D: Nonlinear Phenomena* **139** 247–275
- [53] Kopidakis G and Aubry S 1999 *Physica D: Nonlinear Phenomena* **130** 155–186
- [54] Bickham S R, Kiselev S A and Sievers A J 1993 *Physical Review B* **47** 14206
- [55] Cretegny T, Dauxois T, Ruffo S and Torcini A 1998 *Physica D: Nonlinear Phenomena* **121** 109 – 126
- [56] Kosevich Y and Lepri S 2000 *Phys. Rev. B* **61** 299–307
- [57] Kabsch W 1976 *Acta Crystallographica* **A32** 922–923
- [58] Tsironis G P and Aubry S 1996 *Phys. Rev. Lett.* **77** 5225–5228
- [59] Piazza F, Lepri S and Livi R 2003 *Chaos* **13** 637
- [60] Moritsugu K, Miyashita O and Kidera A 2003 *J. Phys. Chem. B* **107**
- [61] Moritsugu K, Miyashita O and Kidera A 2000 *Phys. Rev. Lett.* **85**
- [62] Lazarides N, Tsironis G P and Kivshar Y S 2008 *Physical Review E* **77** 065601
- [63] Mirny L and Shakhnovich E 2001 *Journal of Molecular Biology* **308** 123–129
- [64] Moritsugu K, Miyashita O and Kidera A 2000 *Phys. Rev. letters* **85** 3970–3973
- [65] Tsai C J, Del Sol A and Nussinov R 2009 *Molecular Biosystems* **5** 207–216
- [66] Gunasekaran K, Ma B and Nussinov R 2004 *Proteins: Structure, Function, and Bioinformatics* **57** 433–443 ISSN 1097-0134